ChemElectroChem

Research Article
doi.org/10.1002/celc.202200514

Chemistry Europe
European Chemical Societies Publishing

www.chemelectrochem.org

Special Collection

Heating up the OER: Investigation of IrO_2 OER Catalysts as Function of Potential and Temperature**

Steffen Czioska,*[a, b] Konrad Ehelebe,[c, e] Janis Geppert,[d] Daniel Escalera-López,[c] Alexey Boubnov,[a] Erisa Saraçi,[a, b] Britta Mayerhöfer,[c, e] Ulrike Krewer,[d] Serhiy Cherevko,[c] and Jan-Dierk Grunwaldt*[a, b]

Despite intensive investigations for unravelling the water splitting reaction, the catalyst behavior during the oxygen evolution reaction (OER) is still not fully understood. This is especially true under more demanding conditions like high potentials and high temperatures. Rotating disk electrode measurements show a gradual increase of OER current when increasing the temperature up to 80 °C. However, strong bubble formation at elevated temperatures makes *in-situ* characterization of the catalyst challenging. Here we utilize an *in-situ* electrochemical and heated flow cell, which aims at an efficient removal of bubbles from the catalyst surface and enables structural studies by X-ray absorption spectroscopy (XAS) at temperatures up to 80 °C. Changes in the Ir L_3-edge X-ray absorption near edge spectra (XANES) were observed with respect to the white line position and principal components related to structural changes were extracted. At temperatures of 60 °C and above, the white line position of XANES spectra reaches a steady state, which is possibly caused by an equilibrium of different Ir oxidation states. These findings provide first spectroscopic insights in the behavior of OER catalysts at elevated temperatures which are typical for industrial applications and rarely addressed until now.

Introduction

Green hydrogen produced by water electrolysis is considered as one of the most promising energy carrier solutions that compensates for the intermittent nature of renewable energies.[1] One of the major technologies for the production of green hydrogen are proton exchange membrane water electrolyzer cells (PEMWE), owing to the high current densities which can be reached.[2] PEMWE cells are already commercially established and are assumed to become more widespread in the near future, working commonly under optimized conditions at 80 °C.[3] The electrochemical water electrolysis reactions in PEMWE cells consist of the hydrogen evolution reaction (HER) at the cathode and the oxygen evolution reaction (OER) at the anode. The bottleneck of the overall reaction is the OER. Hereby, OER catalyst materials are often composed of scarce and expensive Ir, its oxides or binary alloys.[4] Besides a high catalytic activity, efficient catalysts also require sufficient stability.[5] This stability has to be particularly guaranteed under fluctuating conditions, which might lead to structural changes.[6]

In order to design efficient electrocatalysts, understanding structural changes and the origin of instability, especially under dynamic operating conditions, is key. In most of the cases, the studies are conducted only close to real operating conditions, such as in X-ray photoelectron spectroscopy,[7] Raman spectroscopy,[8] and electron microscopy.[7b,9] *Operando* X-ray absorption spectroscopy (XAS) and related techniques are valuable tools for observing structural changes on the electrocatalyst during operation.[10] Factors hampering *in-situ* X-ray transmission studies are the bubble evolution on the HER and OER catalysts, especially at elevated overpotentials, which interferes with spectroscopic data collection and makes the acquisition of quality spectra challenging. In fact, only recently *in-situ* XAS measurements were performed at potentials above 1.5 V vs. the reversible hydrogen electrode (RHE).[11] The measurements were conducted in an *in-situ* XAS electrochemical cell at room temperature. High quality data was obtained due to the use of special conditions coupled with the combined data approach of several XAS methods. Especially the utilization of quick-scanning XAS (also called QEXAFS[12]), made it possible to acquire XAS spectra at a high rate. However, this method

[a] Dr. S. Czioska, Dr. A. Boubnov, Dr. E. Saraçi, Prof. Dr. J.-D. Grunwaldt
Institute for Chemical Technology and Polymer Chemistry, Karlsruhe Institute of Technology, Germany
E-mail: steffen.czioska@kit.edu
grunwaldt@kit.edu
[b] Dr. S. Czioska, Dr. E. Saraçi, Prof. Dr. J.-D. Grunwaldt
Institute of Catalysis Research and Technology, Karlsruhe Institute of Technology, Germany
[c] K. Ehelebe, Dr. D. Escalera-López, Dr. B. Mayerhöfer, Dr. S. Cherevko
Helmholtz-Institute Erlangen-Nürnberg for Renewable Energy (IEK-11), Forschungszentrum Jülich GmbH, Erlangen, Germany
[d] J. Geppert, Prof. Dr.-Ing. U. Krewer
Institute for Applied Materials – Electrochemical Technologies, Karlsruhe Institute of Technology, Germany
[e] K. Ehelebe, Dr. B. Mayerhöfer
Friedrich-Alexander-Universität Erlangen-Nürnberg, Department Chemie- und Bioingenieurwesen, Germany

[**] OER: oxygen evolution reaction

Supporting information for this article is available on the WWW under https://doi.org/10.1002/celc.202200514

Special Collection
This publication is part of a joint Special Collection with ChemCatChem on "Catalysts and Reactors under Dynamic Conditions for Energy Storage and Conversion (DynaKat)". Please check our homepage for more articles in the collection.

needs high X-ray flux and this is rarely implemented as it is available only at few synchrotron sources.[12] Our previous study showed that principal component analysis (PCA) can be used to extract specific components that are related to different reaction modes.[11] In contrast to results at lower potentials, the work showed like in few other studies reported[13] that at potentials beyond 1.5 V vs. RHE the white line (WL) position was moving to lower energies, indicating a seemingly reduction of the catalyst. This was rationalized by the more rapid removal of oxygen from the lattice, which then led to an increased Ir–Ir interaction and shows the need for further studies at high electrode potentials. Since then, also other explanations were put forward.[14]

Stronger bubble evolution due to higher electrochemical activity at elevated temperatures makes spectroscopic investigation of PEMWE catalyst even more demanding. Therefore, XAS studies on electrolyzer systems are still mainly conducted at room temperature,[13a,15] limiting the view into more realistic systems which operate optimally at higher temperatures.

Herein, we present the challenges of using a conventional beamline and the related data analysis for *in-situ* XAS investigations of OER catalysts. The electrochemical *in-situ* XAS cell utilized was based on the design from Binninger et al.[16] and modified to enable measurements at elevated temperatures and ambient pressure. Another goal of this study was to conduct XAS measurements of OER catalysts at a conventional XAS beamline, previously only reported at sophisticated QuickXAS lines.[11] We performed the studies on a flame-spray derived and calcined IrO_2 sample and report on structural studied by Ir L3-XAS at 0.6 to 1.6 V. Apart from measurements at high potentials, the aim of this study was to reveal the temperature dependence of the catalyst at 20, 40, 60 and 80 °C.

Results and Discussion

Method Validation at Room Temperature

The electrochemical and heated *in-situ* cell was connected to a system of several devices to ensure optimized operation, as shown in Figure 1. A peristaltic pump was used to deliver the electrolyte, whilst the temperature of the electrodes and electrolyte was controlled and monitored continuously and was kept stable throughout the measurements. Besides the XAS measurements presented here in the transmission mode, it is also possible to acquire data in the fluorescence mode.

The catalyst nanoparticles were characterized by X-ray diffraction (XRD) and transmission electron microscopy (TEM) (Figure 1). The diffraction peaks fit exactly the characteristic diffractogram of rutile IrO_2, and the synthesized particles also showed a good crystallinity with small size distribution. For a more detailed characterization we refer to our previous publications.[11,17]

Our earlier measurements[11] on IrO_2 during the OER at high overpotentials showed some material degradation and reduction at >1.5 V. In this case quick-scanning XAS was used, which enabled averaging out spectral distortions occurring in a relatively small fraction to the large number of spectra collected, e.g., 600 scans averaged over 10 minutes during steady-state operation. The main findings of that study were a shift in the Ir L_3-edge white line position indicating a change in the adsorbed intermediates on the IrO_2 surface, as well as the decrease of the white line intensity. The latter suggested a partial surface reduction due to a high number of oxygen vacancies. Two principal components were extracted which directly related to these two changes.

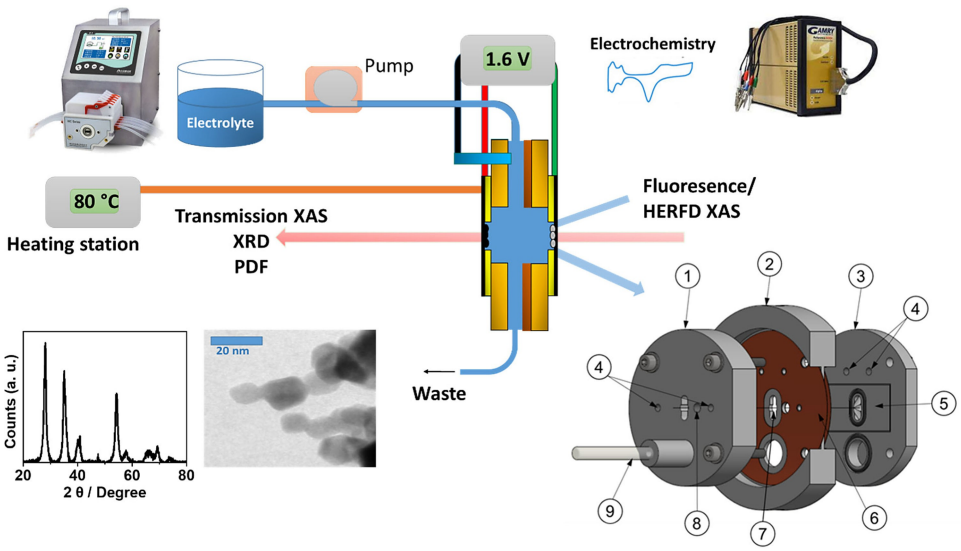

Figure 1. Schematic overview of the experimental set up with basic XRD and TEM characterization of the here investigated particles and schematic view of the heated OER cell for spectroscopy with an explanatory sketch on the left and cross section. (1) Working electrode side flange, (2) flow cell body, (3) counter electrode side flange, (4) threaded boreholes for spring contacts, (5) area for placing counter electrode; corresponding area exists on working electrode flange, (6) Kapton-encapsulated heating foil, (7) electrolyte compartment and X-ray window, (8) threaded borehole for thermocouple, (9) reference electrode, (10) electrolyte inlet.

In this study we now used the easier accessible conventional continuous scanning extended X-ray absorption fine structure (EXAFS) setup (2 min/scan) to obtain analyzable spectra by averaging over many scans, despite the occasional distortions by sudden change in X-ray absorption due to bubble formation. Increasing the scan time per spectrum further, e.g., 20–40 minutes in step-scanning mode, decreased the spectra quality significantly to the point that the data could not be used.

For the room temperature measurements, we recorded 30 X-ray absorption near edge spectra (XANES) over 1 hour at each experimental condition (temperature and potential) with 2 minutes per spectrum (cf. Figure 2). Despite the electrolyte flow, bubble evolution showed strong signal disturbance by change in X-ray absorption in several spectra. Bubble evolution was especially strong with increasing temperature. As a representative example, room temperature measurements acquired during the OER at 1.5 V (Figure 2A) show that only few spectra present strong distortion due to bubble evolution; conversely, most spectra recorded at the same applied potential (Figure 2B) at 60 °C show clear distortions.

To access also data at elevated temperatures and elevated voltages, we had to establish a data conversion approach. Besides the shortening of the measurement time (Figure 3A) and the collection of several lower quality spectra instead of one high quality spectrum with longer measurement time, the most distorted spectra were identified and discarded (cf. scheme of data analysis and result in Figure 3B). Discarding spectra can potentially modify the resulting averaged spectra. Therefore we checked whether the white line position was completely stable within the spectral series, which was confirmed. Hence, this procedure allowed safe removal of distorted spectra without losing essential information on the catalyst structure. In a last step, the resulting spectra were averaged to further remove minor distortions (Figure 3C). While this method generates good analyzable data in the XANES region, we cannot guarantee sufficiently high data quality in the EXAFS region. Hence, we did not analyze the EXAFS part of the collected data in this publication (further procedures like deglitching and step removal should be conducted in this case). In the following section, the temperature-dependent experiment and results obtained by this analysis method will be presented.

Temperature-Dependence of OER Performance and Catalyst Structure

Elevated temperatures are commonly applied in commercial electrolyzers but are seldomly investigated in spectroscopic studies. For assessing how increased electrolyte temperature affects OER activity, we performed temperature-dependent

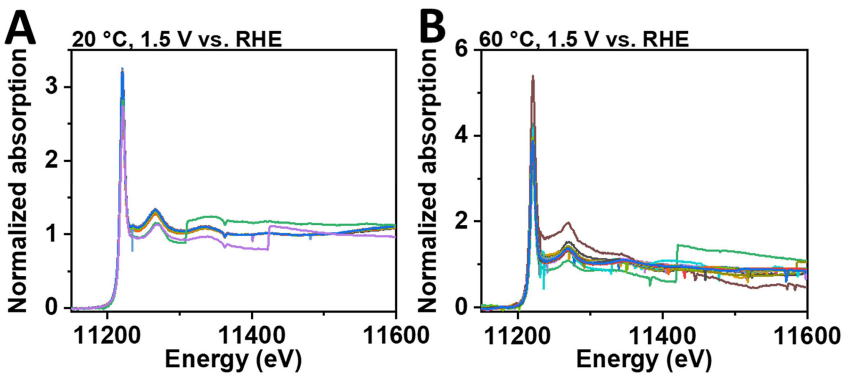

Figure 2. Measured spectra to illustrate signal disruption due to bubble evolution. Different colors relate to repeated scans under the same conditions. The spectra were taken at 20 °C (A) and at 60 °C (B), with an applied potential of 1.5 V for each.

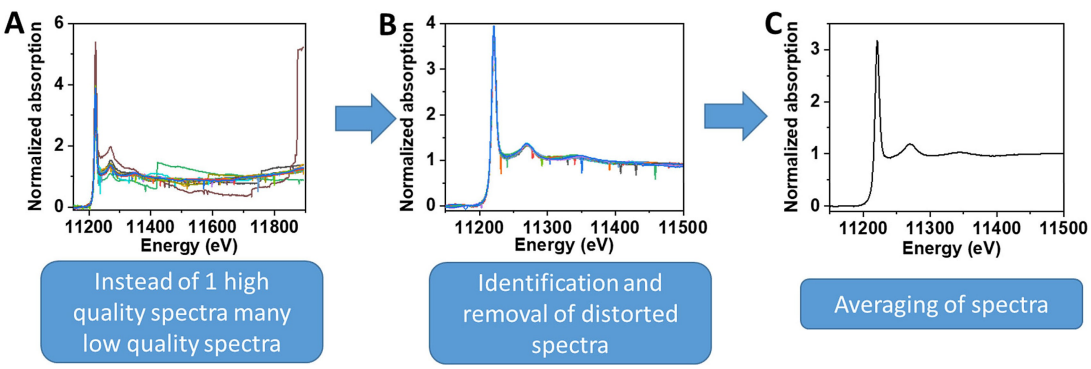

Figure 3. Scheme of data analysis at 60 °C at 1.5 V vs. RHE. All 30 measured spectra (A), sorted spectra (B, 22 remaining) and averaged spectra (C).

experiments in a rotating disk electrode setup (RDE) which are shown in Figure 4A. To better resolve the redox peaks, a fast scan rate of 200 mV/s was applied. The measurements show a gradual increase of OER current when increasing the temperature from 20 to 40 to 60 and to 80 °C, which is due to the rate increase of the catalytic reaction at higher temperature. Pre-OER peaks which are related to absorbed species also move to lower potential values due to the excess thermal energy which is added to the applied electrochemical energy (Figure 4B). Figure 4C shows the positions of the peaks, which confirms the trend for each respective peak with temperature.

In order to investigate this effect of temperature on the catalyst performance, we collected XAS spectra at 20, 40, 60 and 80 °C (Figure 5) during OER at varying potentials (0.6–1.6 V). We were able to collect good quality spectra at room temperature (20 °C) (see Figure 5A). While the spectra at potentials lower than 1.5 V showed no influence of bubbles, at higher potential some disturbances are observable due to the change in X-ray absorption. A shift of the white line to higher energy with increasing potential from 0.6 to 1.5 V vs. RHE is visible (Figure 5A). Then, at 1.6 V vs. RHE, a decrease was observed. This can be related to the formation of oxygen vacancies.[11] Additionally, recent complementary microkinetic models showed that this effect can also be related to a change in absorbed species.[18]

Principal component analysis (PCA) was then performed, which yielded three relevant components (Figure 6). They directly correlate to the different processes as described in the following, in agreement with previous findings.[11] Figure 6A shows all three principal components, of which component **1** represents the general background of the spectra and is related to the part of the catalyst which remains unaltered throughout the experiment. Components **2** and **3** are shown magnified in Figure 6B. Despite of some noise in the spectra, the distinct shape of the principal components could be clearly identified, as previously depicted.[11] While the shape of component **2** can

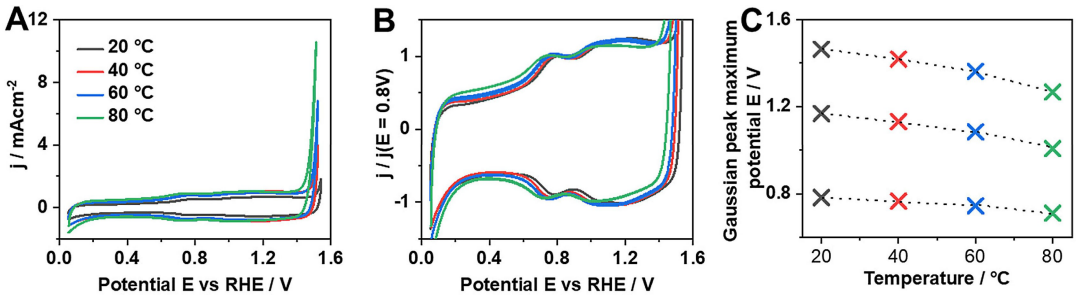

Figure 4. Electrochemical RDE measurements at different temperatures. Cyclic voltammograms (A) with a magnified view on the pre OER peaks normalized at 0.8 V (B) and progression of anodic values of these peaks with temperature (C). Measurements were performed in 0.1 M H_2SO_4 with a scan rate of 200 mV/s.

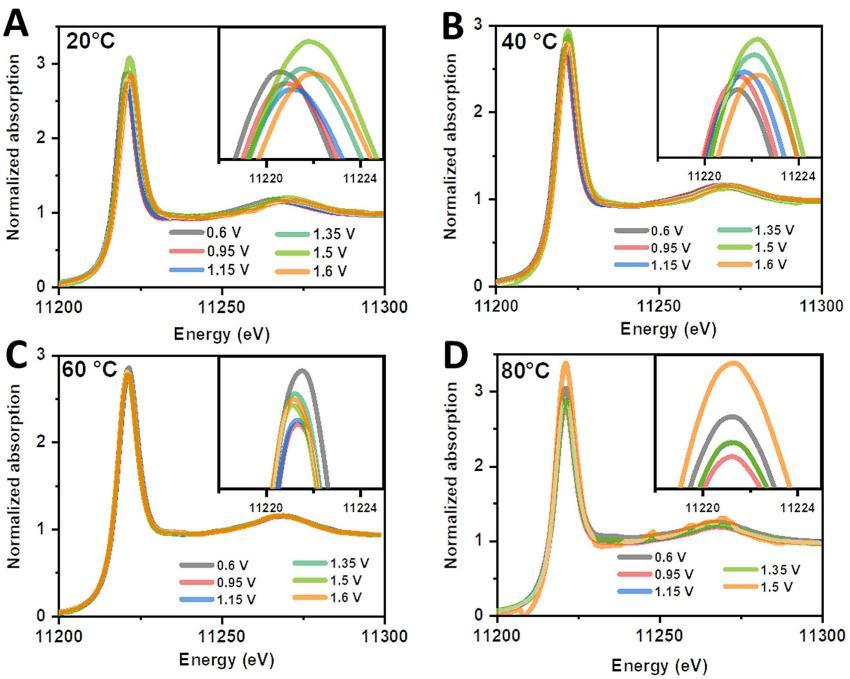

Figure 5. XAS spectra of IrO_2 at the IrL_3-edge during OER at different temperatures and potentials with magnified white line in the inset (data were smoothed by a spline, original data given in the electronic support information, cf. Figure S1). (Note that at 80 °C, the spectra at 1.15 V and 1.35 V are overlaying, see also ESI)

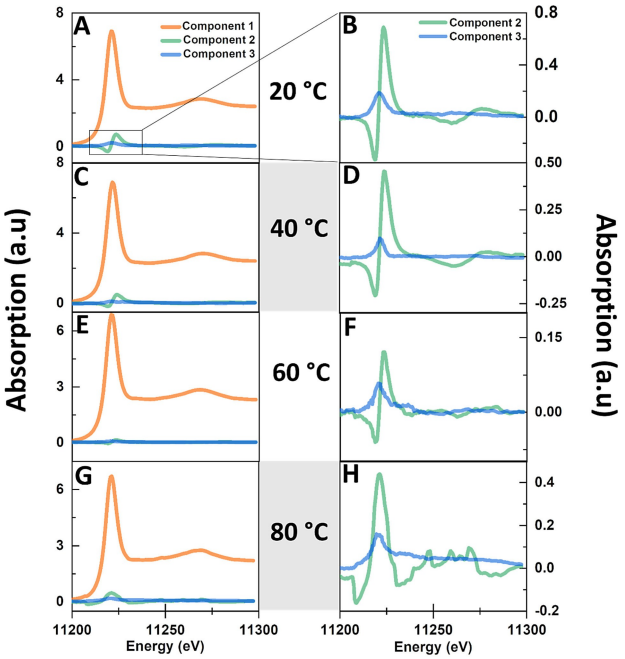

Figure 6. Principal component analysis of Ir L_3-XAS spectra of IrO_2 during OER at 20 °C (A), 40 °C (C), 60 °C (E) and 80 °C (G) and with corresponding magnified segment of components **2** and **3** shown in (B, D, F, H).

be correlated to a standard AEM (adsorbate evolution mechanism) mode indicating a change in adsorbed intermediate species, component **3** can be associated with the formation of oxygen vacancies.

Next, we aimed at investigating the influence of temperature on the IrO_2 catalysts by in-situ XAS. Despite the importance of elevated temperatures for commercial applications of PEMWE, *in-situ* investigations above 20 °C are rare due to technical complexities. In a first step, we increased the temperature to 40 °C and employed the same electrochemical protocol as described above. Despite of the increased bubble formation at 40 °C compared to room temperature, the quality of the data acquisition could be preserved (Figure 6B). The principal components show the same features as at 20 °C, suggesting that at a modest increase in temperature, the processes were unchanged.

Once the cell was heated further to 60 °C, the XAS data quality remained sufficiently high, but the spectra changed slightly in shape (Figure 5C), which was also reflected in the calculated PCA components in Figure 6F. Both components **2** and **3** for 60 °C resemble components **2** from the measurements at 20 °C and 40 °C, (Figure 6B and D), but show stronger noise contributions. The additional energy input within the system induced by the elevated temperatures might change the adsorbed intermediate species or the kinetics of different reaction steps. Given the sufficiently high data quality obtained (Figure 5C) and the fact that the main features of the PCA components were extracted from the white line region (around 11220–11240 eV), for which we assume high accuracy, the observed component changes do not seem to be related to artifacts of the data acquisition.

In contrast, the measurements at further elevated temperatures (80 °C) presented vigorous O_2 gas evolution, resulting in very noisy spectra which did not provide conclusive results at high OER potential values (1.6 V). It was clearly observed that the perturbations in the XAS spectra increased with increasing temperatures which is directly correlated to the stronger bubble evolution caused by faster OER kinetics. Due to the compromised data acquisition, and the spectral quality as shown in Figure 6D, we speculate that the shape distortion of the PCA components in Figure 6H is directly related to the spectral distortion observed during measurements.

For a closer look at the effect of temperature on the white line, the spectra at 1.5 V were displayed together for comparison (Figure 7). This potential was chosen because it was the highest potential for which data acquisition was possible at all temperatures. In addition, because we expect that the contribution of the active catalytic species at 1.5 V to be stronger than at lower potentials and therefore changes in the spectra for different temperatures can be more strongly linked to changes in the active sites. It can be observed that the white line maximum (11221.9 eV) is first shifted to higher energy from 20 °C to 40 °C (11222.2 eV), indicating an oxidation of the catalyst surface. The white line position is then shifted to lower energies from 40 °C to 60 °C (11220.8 eV) and then to 80 °C (11220.8 eV). This indicates that the change in Ir oxidation state responsible for the white line shift also depends on the temperature. A temperature dependence of oxidation state or predominant species at the surface is indeed to be expected assuming an Arrhenius behavior with different energies for the individual reactions; a similarly strong change of oxidation state and predominant species has been shown for the potential dependence.[19]

By comparing the white line position for each temperature at different OER potentials, similar results as in the literature were observed,[11] which validates the approach in this study and also confirms that Ir is partially reduced at elevated potentials (Figure 8). More specifically, from 0.6 V up to 1.5 V versus RHE, the white line shows an oxidation of Ir species up

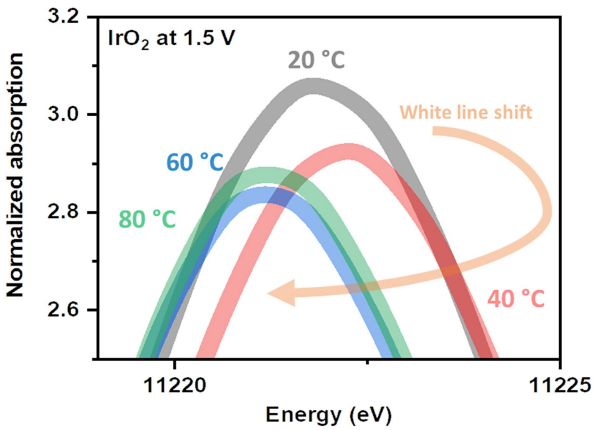

Figure 7. Magnified white line position of the Ir L_3-XANES of IrO_2 during OER at 1.5 V at different temperatures. The arrows indicates the trend of the white line change (data were smoothed by a spline, original data given in the electronic support information, cf. Figure S2).

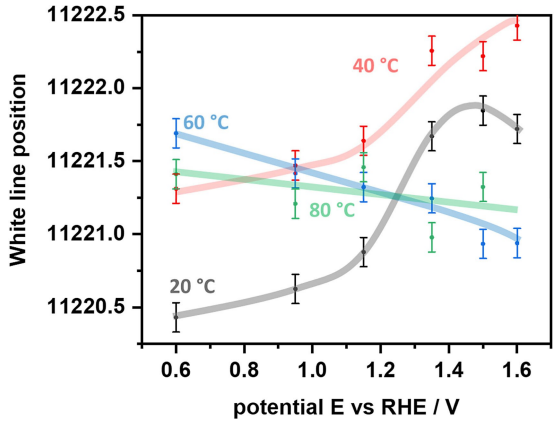

Figure 8. Dependence of white line position of IrO_2 relative to applied potential during OER at different temperatures. The error bars indicate half of the energy resolution of 0.2 eV.

to 1.5 V, followed by a reduction at 1.6 V, which can be related to the formation of oxygen vacancies.[11] Another study hypothesized that this effect is linked to a high beam flux.[14b] It was proposed that high flux rates might heat up the catalyst locally, unintentionally changing the material. However, on the one side, if this effect is caused by heating, it will also commonly appear in commercial electrolyzers and is therefore important to be further investigated. On the other side, the beamflux utilized here is significantly lower than what was suggested to prevent this effect. Beyond such effect, it is worth noting that mass transport and other phenomena can come into play in such anode materials which are important to study in such realistic samples.[20]

At 40 °C the white line showed a similar trend as at a temperature of 20 °C. At a potential of 0.6 V, the energy of the white line position lies higher, indicating that at this temperature the IrO_2 catalyst is in a more oxidized state. With increasing potential, the catalyst is then further oxidized. In contrast, the reduction at a high potential of 1.6 V is not observed. This indicates that the origin of the observed reduction at high potentials at 20 °C needs further attention.

At 60 °C and 80 °C, the white line at a low potential of 0.6 V is higher than for 20 °C and 40 °C, indicating that due to the higher temperature, the catalyst is more oxidized. When increasing the applied potential, the white line only moved slightly, decreasing by a small margin, which can also be a temperature effect. The rather stable oxidation state is unexpected since an increase in potential should theoretically induce a strong increase in the electrochemical potential which would further oxidize the electrocatalyst.

This indicates that at elevated temperatures a stationary equilibrium of different Ir-oxidation states is established, probably between Ir^{3+} and Ir^{4+} species[21] (and probably Ir^{5+})[7a,e] which is stable in the potential range applied here. XAS only measures the average oxidation state. At increasing OER potentials, this equilibrium only changes slightly.

A possible explanation might lie in the temperature dependence of water adsorption and dissociation. The potential-independent water sorption, which was predicted by kinetic modeling to hamper the OER at high potentials,[18,19] would be significantly increased at high temperatures, leading to strongly different prevailing species at the surface than at room temperature. Therefore, at temperatures above 40 °C, water absorption and dissociation, might take place at lower potentials; indeed, a decrease in the kinetic activation energies for the OER with increasing temperature was observed for IrO_2 and other OER electrocatalyst materials.[22] Such accelerated water dissociation kinetics would also justify the performance increase in Figure 4 leading to changes in the surface adsorbate species population as well as the surface oxidation states, as oxygen evolution takes place at higher rate. Previously, at high reaction rates and room temperature, oxygen vacancy refilling was kinetically limiting, causing rearrangements in the lattice and influencing white line position, interpreted as increased Ir–Ir interactions.[11] Here, with increasing the temperature, a vacancy formation-refilling equilibrium might be reached by oxygen vacancies being refilled directly, without the lattice rearrangement and the related white line position shift.

An alternative explanation might be that above 40 °C, the absorbed species are similar in nature to the adsorbates formed during the OER. The system would then already at lower potentials have enough energy to form them without the proceeding oxygen evolution.

The processes that occur at these elevated temperatures are too fast to observe with the method applied here as it averages all species present on the catalyst. Therefore, methods with higher time resolution might be utilized in future studies to better investigate the phenomena reported here.

In future, the cell design should be altered as well with the aim that possible mass transport effects are minimized and the effect of bubbles by the oxygen evolution is tackled, a topic that has been recently put forward as "understanding the transport nexus in electrolysis" in a perspective article.[20] Notably, a recent study showed a strong discrepancy of catalyst stability between aqueous laboratory and PEMWE systems,[23] which should be addressed by future *in-situ* investigations to gain application relevant results. This could be either achieved by the stepwise addition of PEMWE building blocks to existing *in-situ* cells or by the modification of already existing PEMWE systems to enable such measurements.

Conclusion

This study shows that it is important to probe the structure of OER catalysts not only at room temperature but also elevated temperatures including at high potentials to fully understand the behavior of the electrocatalysts under technically relevant conditions. For this purpose a modified in-situ cell was utilized that enabled operating at working temperatures in the range between 20 °C and 80 °C. At these elevated temperatures, strong bubble evolution is challenging for data acquisition, especially under higher OER potentials. Sufficiently high data quality up to 60 °C was reached, while at 80 °C distortion of the measured signal due to strong bubble evolution was observed.

At elevated temperatures above 40 °C, a steady state of the white line position was observed. This is probably related to a stable oxidation state of Ir at these temperatures which is only slightly changed in the potential window applied here.

The here presented results can be further extended to allow for a better understanding of the OER under high overpotentials and elevated temperatures also for other electrocatalysts, and to especially understand catalyst behavior under industrially relevant conditions.

Experimental Section

Rotating Disc Set-up (RDE) Measurements

Cyclic voltammetry measurements were carried out on a Gamry 3000 potentiostat (Gamry Instruments) using a Teflon cell and a modulated speed rotator (MSR) electrode rotator (Pine Research) equipped with a glassy carbon working electrode (ø 5.0 mm) coated with IrO_2 nanoparticle catalysts (synthesis see below). A platinum wire was used as counter electrode. The potentials were normalized to a RHE reference electrode (Hydroflex, Gaskatel GmbH). A 0.1 M aqueous acidic H_2SO_4 electrolyte was used for all electrochemical experiments. The electrolyte temperature was adjusted to 20, 40, 60 and 80 °C using a heating plate. Before each measurement, the solution was purged with argon (99.999%, Air Liquide). Freshly polished glassy carbon working electrodes were used for drop-casting catalyst ink. The IrO_2-containing catalyst ink was prepared as follows: 2.0 mg of IrO_2 nanoparticles, 8.58 µL of Nafion 5% in H_2O/isopropanol (w/w) (D520, VWR), and 1.2 µL of 1 M KOH (pH adjustment to ca. 11) were dispersed in 250 µL of isopropanol and 750 µL of deionized H_2O (> 16.2 MΩ). The mixture was sonicated for 10 min and another 5 min before each drop-casting. Subsequently, 10 µL of ink were drop-casted onto the electrode and dried at 60 °C for at least 30 min, yielding a catalyst loading of 0.1 $mg_{catalyst}\,cm_{geom}^{-2}$. Potentials were *iR* corrected after the experiment, with the electrolyte resistance extracted from electrochemical impedance spectra.

Electrochemical Cell

An *in-situ* OER cell has been built that allows heating to study the structure of catalysts during the OER from 20 to 80 °C. The cell is a modified version of a cell reported by Binninger et al.[16] The construction of the cell is as follows (Figure 1): the cell is build up out of three main parts, the working electrode side flange (1), the flow cell body (2) and the counter electrode side flange (3), which are assembled to form the main body. The boreholes (4) in this structure serve to enable an electrical contact of working and counter electrodes (5) with the potentiostat. To allow measurements at elevated temperatures, the basic construction was supplemented by a flexible Kapton-encapsulated resistive heating foils (6) attached to one or both sides of the electrolyte compartment. This allows for homogeneous heating for both the working and counter electrode, as well as the flowing electrolyte. The temperature was controlled with a K-type thermocouple (8) in contact with the working electrode. The electrolyte inlet (10) first connects the reference electrode (Ag/AgCl, BASi Research Products) (9) compartment and then with the flow through the X-ray window (7) to prevent a connection interruption between the three electrodes due to bubble evolution, similarly as reported by Binninger et al.[16]

Catalyst Synthesis and Characterization

The IrO_2 nanoparticle catalysts were synthesized by flame spray pyrolysis (FSP),[24] as recently reported by our group.[17] In short, 1 g of iridium acetylacetonate (iridium(III) 2,4-pentanedionate, Ir 37.5% min, Alfa Aesar) was dissolved in a mixture of 25 mL concentrated acetic acid and 25 mL methanol. The solution was then placed into an ultrasonic bath for 1 h to ensure full dissolution of the precursors. Subsequently, the resulting solutions were filled into a 50 mL syringe (Hamilton syringes, KF6, gauge 22) and set into a syringe pump (Legato 210, KD Scientific Inc.).[25] The solution was injected with a flow rate of 5 mL min^{-1} and dispersed with 5 NL min^{-1} oxygen gas flow at 3 bar back-pressure while being released through a steel capillary of 0.413 mm diameter into the FSP chamber. A supporting flame of 0.75 NL min^{-1} methane and 1.6 NL min^{-1} oxygen flow was used to ignite the dispersed solution. The synthesized particles were collected in a cylindrical filter holder 80 cm over the flame by a glass fiber filter (Whatman GF6, GE) connected with a vacuum pump (R5, Busch). Water cooling was used to prevent the nozzle from overheating and to keep the fiber filter at a low temperature. After collection, the as-prepared catalysts were placed in a calcination furnace and heated up to 600 °C in air (2 h, 2 °C min^{-1} heating ramp). The particles were then characterized by an FEI Titan 80–300 transmission electron microscope (TEM) operated at a 300 kV acceleration voltage in a high-angle annular dark-field scanning mode to study particle size and morphology. X-ray diffraction (XRD) patterns were acquired using a Bruker D8 Advance diffractometer using Cu Kα radiation (λ = 1.54 Å, an accelerating electron voltage of 40 kV, an anode current of 35 mA). The intensity of scattered X-rays was measured in a 2θ-range of 20–90°, a step width of 0.0164°, 1 step s^{-1}. For a more in-depth characterization of the same particles see the previous publications.[11,17]

Preparation of Electrodes

The catalyst was fixed on Kapton paper and used as working and counter electrodes, similar to a previous approach.[11] In short, the Kapton paper electrodes were fixed on a heating plate, covered with a Teflon mask to define the area of catalyst coating, and heated to 80 °C to facilitate ink drying. The ink was then spray coated on the Kapton paper and after drying used directly as working and counter electrodes. For the ink preparation and catalyst coating see details in ref.[10a] All working electrodes had an iridium oxide loading between 2 and 3 mg/cm^2.

X-Ray Absorption Spectroscopy (XAS) Measurements

In-situ XAS measurements were performed at Karlsruhe Institute of Technology (KIT) light source at the CATACT wiggler beamline[26] using a Si(111) double-crystal monochromator, with Rh mirrors for harmonic rejection. Intensity before and after the sample were measured by ion chambers (Oxford), filled with mixtures of nitrogen and argon. The XAS data were recorded at the Ir L_3-edge (11215 eV) in transmission mode from 11000 to 11900 eV and using Pt foil as reference (2 min/scan), with a maximum photonflux of 10^{11} photons/s ×100 mA, with around a fourth of this used during measurements. Data was collected at 20, 40, 60 and 80 °C during OER at varying potentials (0.6–1.6 V vs. RHE). The potentials were measured vs. Ag/AgCl and converted vs. RHE taking in regard the temperate influence on the potential according to the Nernst equation (Eq.1):

$$E = E^0 + \frac{RT}{zF} ln \frac{a_{Ox}}{a_{Red}} \quad (1)$$

Where E is the electrode potential, E^0 is the standard electrode potential, R is the universal gas constant (8.31447 $J mol^{-1} K^{-1}$), T is the temperature in Kelvin, z is the number of exchanged electrodes, F is the Faraday constant (96485.34 C mol^{-1}) and a is the activity of the redox species.

The recorded raw data at the different reaction conditions were then analyzed using Athena and Artemis of the iFEFFIT package.[27] The energies of the spectra were calibrated and aligned using reference Pt metal foil channels to correct any energy shifts, and the spectra were normalized. For each of the spectral series with varying potentials, principal component analysis (PCA) was applied to X-ray absorption near-edge structure (XANES) also by utilizing the Athena[27] software in order to identify the principal (unique) components comprising the data set (For an explanation of PCA on a fundamental level we refer to the experimental section of our previous study[11]).

Acknowledgement

U.K., J.-D.G. and S.C. gratefully acknowledge the DFG for financial support within the grants KR 3850/8–1 (U.K.), GR 3987/15–1 (J.-D.G.) and CH 1763/3–1 (S.C.), as a part of the Priority Program SPP 2080 "Catalysts and reactors under dynamic conditions for energy storage and conversion." The authors acknowledge the KIT Light Source (run by the Institute for Beam Physics and Technology) for providing beamtime at the CatAct-beamline, specifically Dr. Anna Zimina for support during XAS measurements. Dr. Bidyut Bikash Sarma is gratefully acknowledged for assistance during the XAS beamtime. Open Access funding enabled and organized by Projekt DEAL.

Conflict of Interest

The authors declare no conflict of interest.

Data Availability Statement

The data that support the findings of this study are available from the corresponding author upon reasonable request.

Keywords: electrochemistry · iridium oxide · oxygen evolution reaction · X-ray absorption spectroscopy · water splitting

[1] a) K. Ayers, N. Danilovic, R. Ouimet, M. Carmo, B. Pivovar, M. Bornstein, *Annu. Rev. Chem. Biomol. Eng.* **2019**, *10*, 219–239; b) J. A. Turner, *Science* **2004**, *305*, 972–974.
[2] M. Carmo, D. L. Fritz, J. Mergel, D. Stolten, *Int. J. Hydrogen Energy* **2013**, *38*, 4901–4934.
[3] a) O. Schmidt, A. Gambhir, I. Staffell, A. Hawkes, J. Nelson, S. Few, *Int. J. Hydrogen Energy* **2017**, *42*, 30470–30492; b) P. Millet, R. Ngameni, S. A. Grigoriev, N. Mbemba, F. Brisset, A. Ranjbari, C. Etiévant, *Int. J. Hydrogen Energy* **2010**, *35*, 5043–5052; c) P. Millet, N. Mbemba, S. A. Grigoriev, V. N. Fateev, A. Aukauloo, C. Etiévant, *Int. J. Hydrogen Energy* **2011**, *36*, 4134–4142; d) C. V. Pham, D. Escalera-López, K. Mayrhofer, S. Cherevko, S. Thiele, *Adv. Energy Mater.* **2021**, *11*, 2101998.
[4] a) S. Cherevko, S. Geiger, O. Kasian, N. Kulyk, J.-P. Grote, A. Savan, B. R. Shrestha, S. Merzlikin, B. Breitbach, A. Ludwig, K. J. J. Mayrhofer, *Catal. Today* **2016**, *262*, 170–180; b) S. Cherevko, A. R. Zeradjanin, A. A. Topalov, N. Kulyk, I. Katsounaros, K. J. J. Mayrhofer, *ChemCatChem* **2014**, *6*, 2219–2223.
[5] A. Loncar, D. Escalera-Lopez, S. Cherevko, N. Hodnik, *Angew. Chem. Int. Ed.* **2022**, *61*, e202114437.
[6] K. F. Kalz, R. Kraehnert, M. Dvoyashkin, R. Dittmeyer, R. Gläser, U. Krewer, K. Reuter, J. D. Grunwaldt, *ChemCatChem* **2017**, *9*, 17–29.
[7] a) J. J. Velasco-Velez, E. A. Carbonio, C. H. Chuang, C. J. Hsu, J. F. Lee, R. Arrigo, M. Havecker, R. Wang, M. Plodinec, F. R. Wang, A. Centeno, A. Zurutuza, L. J. Falling, R. V. Mom, S. Hofmann, R. Schlogl, A. Knop-Gericke, T. E. Jones, *J. Am. Chem. Soc.* **2021**, *143*, 12524–12534; b) L. J. Falling, R. V. Mom, L. E. Sandoval Diaz, S. Nakhaie, E. Stotz, D. Ivanov, M. Havecker, T. Lunkenbein, A. Knop-Gericke, R. Schlögl, J. J. Velasco-Velez, *ACS Appl. Mater. Interfaces* **2020**, *12*, 37680–37692; c) L. J. Frevel, R. Mom, J.-J. Velasco-Vélez, M. Plodinec, A. Knop-Gericke, R. Schlögl, T. E. Jones, *J. Phys. Chem. C* **2019**, *123*, 9146–9152; d) V. A. Saveleva, L. Wang, W. Luo, S. Zafeiratos, C. Ulhaq-Bouillet, A. S. Gago, K. A. Friedrich, E. R. Savinova, *J. Phys. Chem. Lett.* **2016**, *7*, 3240–3245; e) H. G. Sanchez Casalongue, M. L. Ng, S. Kaya, D. Friebel, H. Ogasawara, A. Nilsson, *Angew. Chem. Int. Ed.* **2014**, *53*, 7169–7172; *Angew. Chem.* **2014**, *126*, 7297–7300; f) R. V. Mom, L. J. Falling, O. Kasian, G. Algara-Siller, D. Teschner, R. H. Crabtree, A. Knop-Gericke, K. J. J. Mayrhofer, J.-J. Velasco-Vélez, T. E. Jones, *ACS Catal.* **2022**, 5174–5184; g) A. A. Permyakova, J. Herranz, M. El Kazzi, J. S. Diercks, M. Povia, L. R. Mangani, M. Horisberger, A. Patru, T. J. Schmidt, *ChemPhysChem* **2019**, *20*, 3120–3127.
[8] a) Y. Mo, I. C. Stefan, W.-B. Cai, J. Dong, P. Carey, D. A. Scherson, *J. Phys. Chem. B* **2002**, *106*, 3681–3686; b) Z. Pavlovic, C. Ranjan, M. van Gastel, R. Schlogl, *Chem. Commun.* **2017**, *53*, 12414–12417; c) K. H. Saeed, M. Forster, J. F. Li, L. J. Hardwick, A. J. Cowan, *Chem. Commun.* **2020**, *56*, 1129–1132.
[9] a) F. D. Speck, M. T. Y. Paul, F. Ruiz-Zepeda, M. Gatalo, H. Kim, H. C. Kwon, K. J. J. Mayrhofer, M. Choi, C. H. Choi, N. Hodnik, S. Cherevko, *J. Am. Chem. Soc.* **2020**, *142*, 15496–15504; b) J. J. Velasco-Velez, R. V. Mom, L. E. Sandoval-Diaz, L. J. Falling, C. H. Chuang, D. Gao, T. E. Jones, Q. Zhu, R. Arrigo, B. Roldan Cuenya, A. Knop-Gericke, T. Lunkenbein, R. Schlogl, *ACS Energy Lett.* **2020**, *5*, 2106–2111; c) J.-J. V. Vélez, Y.-Y. Chin, M.-H. Tsai, O. J. Burton, R. Wang, S. Hofmann, W.-H. Hsu, T. Ohigashi, W.-F. Pong, C.-H. Chuang, *Chin. J. Phys.* **2022**, *76*, 135–144.
[10] a) M. Povia, D. F. Abbott, J. Herranz, A. Heinritz, D. Lebedev, B.-J. Kim, E. Fabbri, A. Patru, J. Kohlbrecher, R. Schäublin, M. Nachtegaal, C. Copéret, T. J. Schmidt, *Energy Environ. Sci.* **2019**, *12*, 3038–3052; b) M. Povia, J. Herranz, T. Binninger, M. Nachtegaal, A. Diaz, J. Kohlbrecher, D. F. Abbott, B.-J. Kim, T. J. Schmidt, *ACS Catal.* **2018**, *8*, 7000–7015; c) K. Ebner, A. H. Clark, V. A. Saveleva, G. Smolentsev, J. Chen, L. Ni, J. Li, A. Zitolo, F. Jaouen, U. I. Kramm, T. J. Schmidt, J. Herranz, *Adv. Energy Mater.* **2022**, *12*, 2103699; d) S. A. Bartlett, E. V. Sackville, E. K. Gibson, V. Celorrio, P. P. Wells, M. Nachtegaal, S. W. Sheehan, U. Hintermair, *Chem. Commun.* **2019**, *55*, 7832–7835; e) B.-J. Kim, E. Fabbri, M. Borlaf, D. F. Abbott, I. E. Castelli, M. Nachtegaal, T. Graule, T. J. Schmidt, *Mater. Adv.* **2021**, *2*, 345–355; f) D. F. Abbott, E. Fabbri, M. Borlaf, F. Bozza, R. Schäublin, M. Nachtegaal, T. Graule, T. J. Schmidt, *J. Mater. Chem. A* **2018**, *6*, 24534–24549; g) J. Ampurdanés, M. Chourashiya, A. Urakawa, *Catal. Today* **2019**, *336*, 161–168; h) F. Dionigi, Z. Zeng, I. Sinev, T. Merzdorf, S. Deshpande, M. B. Lopez, S. Kunze, I. Zegkinoglou, H. Sarodnik, D. Fan, A. Bergmann, J. Drnec, J. F. Araujo, M. Gliech, D. Teschner, J. Zhu, W. X. Li, J. Greeley, B. R. Cuenya, P. Strasser, *Nat. Commun.* **2020**, *11*, 2522; i) A. Dutta, A. Kuzume, V. Kaliginedi, M. Rahaman, I. Sinev, M. Ahmadi, B. Roldán Cuenya, S. Vesztergom, P. Broekmann, *Nano Energy* **2018**, *53*, 828–840; j) T. Möller, F. Scholten, T. N. Thanh, I. Sinev, J. Timoshenko, X. Wang, Z. Jovanov, M. Gliech, B. Roldan Cuenya, A. S. Varela, P. Strasser, *Angew. Chem.* **2020**, *132*, 18130–18139; *Angew. Chem. Int. Ed.* **2020**, *59*, 17974–17983.
[11] S. Czioska, A. Boubnov, D. Escalera-López, J. Geppert, A. Zagalskaya, P. Röse, E. Saraçi, V. Alexandrov, U. Krewer, S. Cherevko, J.-D. Grunwaldt, *ACS Catal.* **2021**, *11*, 10043–10057.
[12] O. Muller, M. Nachtegaal, J. Just, D. Lutzenkirchen-Hecht, R. Frahm, *J. Synchrotron Radiat.* **2016**, *23*, 260–266.
[13] a) D. F. Abbott, D. Lebedev, K. Waltar, M. Povia, M. Nachtegaal, E. Fabbri, C. Copéret, T. J. Schmidt, *Chem. Mater.* **2016**, *28*, 6591–6604; b) E. Oakton, D. Lebedev, M. Povia, D. F. Abbott, E. Fabbri, A. Fedorov, M. Nachtegaal, C. Copéret, T. J. Schmidt, *ACS Catal.* **2017**, *7*, 2346–2352.
[14] a) H. N. Nong, L. J. Falling, A. Bergmann, M. Klingenhof, H. P. Tran, C. Spori, R. Mom, J. Timoshenko, G. Zichittella, A. Knop-Gericke, S. Piccinin, J. Perez-Ramirez, B. R. Cuenya, R. Schlögl, P. Strasser, D. Teschner, T. E. Jones, *Nature* **2020**, *587*, 408–413; b) N. Diklić, A. H. Clark, J. Herranz, J. S.

Diercks, D. Aegerter, M. Nachtegaal, A. Beard, T. J. Schmidt, *ACS Energy Lett.* **2022**, 1735–1740.
[15] a) F. Nattino, N. Marzari, *Phys. Chem. Chem. Phys.* **2020**, *22*, 10807–10818; b) A. H. Reksten, A. E. Russell, P. W. Richardson, S. J. Thompson, K. Mathisen, F. Seland, S. Sunde, *Phys. Chem. Chem. Phys.* **2020**, *22*, 18868–18881; c) A. R. Hillman, M. A. Skopek, S. J. Gurman, *Phys. Chem. Chem. Phys.* **2011**, *13*, 5252–5263.
[16] T. Binninger, E. Fabbri, A. Patru, M. Garganourakis, J. Han, D. F. Abbott, O. Sereda, R. Kötz, A. Menzel, M. Nachtegaal, T. J. Schmidt, *J. Electrochem. Soc.* **2016**, *163*, H906-H912.
[17] D. Escalera-López, S. Czioska, J. Geppert, A. Boubnov, P. Röse, E. Saraçi, U. Krewer, J.-D. Grunwaldt, S. Cherevko, *ACS Catal.* **2021**, *11*, 9300–9316.
[18] J. Geppert, P. Röse, S. Czioska, D. Escalera-Lopez, A. Boubnov, E. Saraci, J.-D. Grunwaldt, U. Krewer, *J. Am. Chem. Soc.* **2022**, *144*, 13205–13217.
[19] J. Geppert, F. Kubannek, P. Röse, U. Krewer, *Electrochim. Acta* **2021**, *380*, 137902.
[20] B. J. M. Etzold, U. Krewer, S. Thiele, A. Dreizler, E. Klemm, T. Turek, *Chem. Eng. J.* **2021**, *424*, 130501.
[21] a) V. Pfeifer, T. E. Jones, S. Wrabetz, C. Massue, J. J. Velasco Velez, R. Arrigo, M. Scherzer, S. Piccinin, M. Havecker, A. Knop-Gericke, R. Schlögl, *Chem. Sci.* **2016**, *7*, 6791–6795; b) V. A. Saveleva, L. Wang, D. Teschner, T. Jones, A. S. Gago, K. A. Friedrich, S. Zafeiratos, R. Schlögl, E. R. Savinova, *J. Phys. Chem. Lett.* **2018**, *9*, 3154–3160; c) V. A. Saveleva, L. Wang, O. Kasian, M. Batuk, J. Hadermann, J. J. Gallet, F. Bournel, N. Alonso-Vante, G. Ozouf, C. Beauger, K. J. J. Mayrhofer, S. Cherevko, A. S. Gago, K. A. Friedrich, S. Zafeiratos, E. R. Savinova, *ACS Catal.* **2020**, *10*, 2508–2516; d) V. Pfeifer, T. E. Jones, J. J. Velasco Velez, R. Arrigo, S. Piccinin, M. Havecker, A. Knop-Gericke, R. Schlögl, *Chem. Sci.* **2017**, *8*, 2143–2149.
[22] a) I. Sohrabnejad-Eskan, A. Goryachev, K. S. Exner, L. A. Kibler, E. J. M. Hensen, J. P. Hofmann, H. Over, *ACS Catal.* **2017**, *7*, 2403–2411; b) E. Nurlaela, T. Shinagawa, M. Qureshi, D. S. Dhawale, K. Takanabe, *ACS Catal.* **2016**, *6*, 1713–1722; c) M. Suermann, T. J. Schmidt, F. N. Büchi, *Electrochim. Acta* **2018**, *281*, 466–471.
[23] J. Knoppel, M. Mockl, D. Escalera-Lopez, K. Stojanovski, M. Bierling, T. Bohm, S. Thiele, M. Rzepka, S. Cherevko, *Nat. Commun.* **2021**, *12*, 2231.
[24] a) W. Y. Teoh, R. Amal, L. Madler, *Nanoscale* **2010**, *2*, 1324–1347; b) L. Mädler, H. K. Kammler, R. Mueller, S. E. Pratsinis, *J. Aerosol Sci.* **2002**, *33*, 369–389.
[25] K. Schuh, W. Kleist, M. Høj, A. D. Jensen, P. Beato, G. R. Patzke, J.-D. Grunwaldt, *J. Solid State Chem.* **2015**, *228*, 42–52.
[26] A. Zimina, K. Dardenne, M. A. Denecke, D. E. Doronkin, E. Huttel, H. Lichtenberg, S. Mangold, T. Pruessmann, J. Rothe, T. Spangenberg, R. Steininger, T. Vitova, H. Geckeis, J.-D. Grunwaldt, *Rev. Sci. Instrum.* **2017**, *88*, 113113.
[27] B. Ravel, M. Newville, *J. Synchrotron Radiat.* **2005**, *12*, 537–541.

Manuscript received: May 13, 2022
Revised manuscript received: August 5, 2022
Accepted manuscript online: August 16, 2022